



Ge, Y., van der Kamp, M., Malaisree, M., Liu, D., Liu, Y., & Mulholland, A. J. (2017). Identification of the quinolinedione inhibitor binding site in Cdc25 phosphatase B through docking and molecular dynamics simulations. *Journal of Computer-Aided Molecular Design*, 31(11), 995-1007. <https://doi.org/10.1007/s10822-017-0073-y>

Peer reviewed version

Link to published version (if available):

[10.1007/s10822-017-0073-y](https://doi.org/10.1007/s10822-017-0073-y)

[Link to publication record in Explore Bristol Research](#)

PDF-document

This is the author accepted manuscript (AAM). The final published version (version of record) is available online via Springer at <https://link.springer.com/article/10.1007%2Fs10822-017-0073-y>. Please refer to any applicable terms of use of the publisher.

University of Bristol - Explore Bristol Research

General rights

This document is made available in accordance with publisher policies. Please cite only the published version using the reference above. Full terms of use are available: <http://www.bristol.ac.uk/red/research-policy/pure/user-guides/ebr-terms/>

Identification of the quinolinedione inhibitor binding site in Cdc25 phosphatase B through docking and molecular dynamics simulations

Short title: Inhibitor binding site identified in Cdc25B

Key words: NSC663284; Docking; Molecular dynamics; binding mode; Protein flexibility

Authors: Yushu Ge ^{1,2#*}, Marc van der Kamp ^{2,3#}, Maturos Malaisree ², Dan Liu ¹, Yi Liu ^{4*},
Adrian J Mulholland ^{2*}

¹ School of Life Sciences, University of Science and Technology of China, Hefei, P. R.
China, 230027

² Centre of Computational Chemistry, School of Chemistry, University of Bristol, Bristol
BS8 1TS, UK

³ School of Biochemistry, University of Bristol, Bristol BS8 1TD, UK

⁴ State Key Laboratory of Virology & Key Laboratory of Analytical Chemistry for Biology
and Medicine (Ministry of Education)&College of Chemistry and Molecular Sciences,
Wuhan University, Wuhan 430072, P. R. China

The work was performed at the Centre of Computational Chemistry, School of Chemistry,
University of Bristol.

These authors contributed equally to this work.

* Corresponding authors:

Prof Yi Liu, Wuhan University, Wuhan 430072, P. R. China E-mail: yiliuchem@whu.edu.cn

Prof Adrian J. Mulholland, University of Bristol, Bristol BS8 1TS, UK. E-mail:

Adrian.Mulholland@bristol.ac.uk

Abstract

Cdc25 phosphatase B, a potential target for cancer therapy, is inhibited by a series of quinones. The binding site and mode of quinone inhibitors to Cdc25B remains unclear, whereas this information is important for structure-based drug design. We investigated the potential binding site of NSC663284 [DA3003-1 or 6-chloro-7-(2-morpholin-4-yl-ethylamino)-quinoline-5, 8-dione] through docking and molecular dynamics simulations. Of the two main binding sites suggested by docking, the molecular dynamics simulations only support one site for stable binding of the inhibitor. Binding sites in and near the Cdc25B catalytic site that have been suggested previously do not lead to stable binding in 50 ns molecular dynamics (MD) simulations. In contrast, a shallow pocket between the C-terminal helix and the catalytic site provides a favourable binding site that shows high stability. Two similar binding modes featuring protein-inhibitor interactions involving Tyr428, Arg482, Thr547 and Ser549 are identified by clustering analysis of all stable MD trajectories. The relatively flexible C-terminal region of Cdc25B contributes to inhibitor binding. The binding mode of NSC663284, identified through MD simulation, likely prevents the binding of protein substrates to Cdc25B. The present results provide useful information for the design of quinone inhibitors and their mechanism of inhibition.

Introduction

Cdc25B, as one of three human isoforms of the cell division cycle (CDC) phosphatase family, is an essential regulator in the cell cycle [1, 2]. It is reported to play an important role in S/G2 (synthesis to gap 2) and G2/M (gap 2 to mitosis) phase transition by dephosphorylating CDK1/cyclin B at the centrosome level [3]. Cdc25B (but not Cdc25A or Cdc25C) is required for checkpoint recovery upon DNA-damage induced arrest of the G2 phase (and subsequent entry into mitosis) [4]. Overexpression of Cdc25 phosphatases in various human cancers is observed and reported, which makes Cdc25B a potential target for anticancer therapy [5-8]. The structure of the catalytic domain of Cdc25B is known [1] and various small molecules have been reported as potent inhibitors of Cdc25B [8-10]. Quinone-based structures are one of the most potent classes of Cdc25B inhibitors observed to date [9, 12]. NSC663284 was one of the quinolinediones first reported as a potential inhibitor ($IC_{50, \text{Cdc25B}}=0.21\mu\text{M}$, see Figure 1) [13]. For many years, the compound has been used as a template to help design new inhibitors and to study the inhibition mechanism [14-16]. Initially, it was suggested that NSC663284 could bind at one of the two anionic binding sites observed in the crystal structures of Cdc25B [12, 17]. In one of the crystal structures determined (PDB ID: 1QB0) [17], this site was identified by a sulfate ion interacting with the P-loop, a loop with the signature sequence HCX₅R that contains the catalytic cysteine and forms part of the catalytic site in all protein tyrosine phosphatases (and thus all Cdc25 phosphatases) [18]. The sulfate ion interacts with residues Arg479, Glu478, Ser477, Ser476, Phe475 and Glu474 [19, 20].

No direct experimental identification of the binding mode of NSC663284 (or other quinone-based inhibitors) to Cdc25B has been reported. A variety of molecular docking studies has studied the binding of NSC663284 and analogues to Cdc25B. Lavecchia *et al.* reported the docking of NSC663284 to the Cdc25B crystal structure using both the AutoDock and Gold programs [21]. AutoDock suggested a network of hydrogen bonds and electrostatic interactions

between the quinone carbonyl oxygens and residues Arg544, Arg482 and Tyr428. In this binding mode, the tail moiety is oriented toward the active site. Gold suggested a very different binding mode, with the quinolinedione ring placed into the active site. The authors suggested that the binding mode found by AutoDock could partially explain the mixed inhibition kinetics and the inhibition mechanism of Cys473 oxidation [22]. Arantes further studied the flexibility of Cdc25B and docked NSC663284 into the crystal structure and into structures obtained from conformational sampling [23]. Binding to the shallow pocket formed beside the P-loop, which is usually called ‘swimming pool’, was observed in docking to several sampled structures, in which the C-terminal helix had been partially unfolded. Several binding orientations were suggested where NSC663284 interacts directly with the P-loop. The author argued that these orientations provide possible explanations for the experimentally observed mixed inhibition kinetics and the irreversible oxidation of the catalytic residue Cys473. It is worth noting that the protein structure is rigid during docking in these previous docking studies [21,22]. Docking studies are also reported for other quinone-based inhibitors. Park H *et al.* reported three different binding modes of NSC 95397, dihydroxyl-NSC 95397 (D-NSC) and fluorinated NSC 95397 (F-NSC) interacting with the P-loop of Cdc25B [24]. Docking of NSC 95397 followed by a single 2.1 ns MD simulation was performed by Ko *et al.* [25]. A shift of the NSC 95397 binding pose was observed during the simulation, and comparison to simulation of the free Cdc25B indicated that the ligand may limit the flexibility of the C-terminal helix. Finally, Braud *et al.* reported a binding mode between a newly synthesized naphthoquinone derivative ([1,4-Dioxo-1,4-dihydronaphthalen-2-yl) methyl] malonic acid) and Cdc25B, in which the naphthoquinone core was placed outside of the P-loop [26].

In summary, previous studies have revealed a range of possibilities for the binding site and binding mode between quinolinedione- and quinone-based inhibitors and Cdc25B. The binding sites identified can be classified as 1) within the catalytic site or 2) within the swimming pool

outside of the P-loop. The suggested binding orientations (or modes) are more varied. All suggested binding modes are obtained with molecular docking programs. It is clear that different programs (employing different algorithms and scoring functions) and/or settings can result in different orientations or even binding sites for the same ligand [27-29]. It is not known which combination of algorithm, scoring function and settings leads to the most reliable prediction of binding to Cdc25B, and it is thus not clear what the likely binding mode of quinolinedione inhibitors is.

In this study, we first use molecular docking to find a variety of initial binding poses of NSC663284 to Cdc25B (using the crystal structure and alternative conformations sampled from MD simulation), and subsequently studied the stability of the main binding modes suggested by docking using extensive MD simulation. The simulations identified one binding site where NSC663284 can bind with relative high stability. Similar interactions between Cdc25B and the ligand are observed during simulations starting from different poses in this binding site. Notably, our results indicate that binding of NSC663284 directly to the catalytic site (P-loop) as reported previously is likely to be unstable [23]. Our simulations and analyses provide new insights into the likely binding site, mode and interactions of quinolinedione inhibitors for Cdc25B, which will assist drug design and pharmacophore studies of quinolinedione-based Cdc25 inhibitors.

Methods

System setup for docking experiments

The structure of NSC663284 (**Figure 1**) was built using SYBYL software package [30]. Geometric optimizations were carried out with the SYBYL/MAXIMIN2 minimizer with the TRIPOS force field (convergence criterion: RMS gradient of forces 0.05 kcal·mol⁻¹ or less).

Crystal structures of cdc25B phosphatase were investigated and compared (table S1). PDB ID 1QB0 [17] was selected for docking and simulation. Compared with the other structures (that are very similar), 1QB0 covers most of the sequence (without any mutations), including coordinates for residues Asp374 to Ala550, as well as the amide nitrogen of Ala551 of the Cdc25B primary sequence. The resolution is reasonably high (1.9 Å). Protonation states were investigated using the H++ Server [31]. Cys473 was predicted to be in the thiolate form. Four histidine residues (His375, His395, His519 and His533) were protonated at N ϵ and two histidine residues (His436 and His472) were protonated at N δ , according to the Optimal Hydrogen Bonding Newtork (as determined using the WHAT-IF server, <http://swift.cmbi.ru.nl/servers/html/index.html>). All other residues were configured in their standard protonation states at pH 7.

Docking of NSC663284 and clustering

Two docking programs were used: AutoDock Vina and AutoDock 4.2 [32-34]. AutoDockTools 1.5.6 was used to prepare the input files. The grid box was centred on the SG atom of Cys473 with a size that allowed the ligand to be docked up to 11 Å (small grid box) and 18 Å (large grid box) away from the catalytic residue Cys473. The ligand and protein prepared as described above were imported, and non-polar hydrogens were merged. Partial charges calculated with the Gasteiger-Marsilli method using SYBYL were used for the ligand. Kollman partial charges were assigned to the protein. Docking with AutoDock Vina was performed with the default parameters. For AutoDock 4.2, exhaustive docking was performed in the small grid box (60 points of 0.375 Å spacing in each dimension) by using a population of 1500 and performing 1000 Lamarckian Genetic Algorithm (GA-LS) runs. The maximum number of generations and energy evaluations were set as 2.7×10^4 and 2.5×10^6 respectively. The 1000 poses generated were clustered according to root mean-squared deviation (RMSD) of the ligand heavy atoms with a 4.0 Å cut off. For the 7 clusters with the highest population,

the coordinates of the conformations with the lowest predicted binding energy were used for further MD simulation. Since the binding pose in the 11st highest populated cluster was similar to that reported previously by Lavecchia *et al.* (using Gold as the docking program) [20], coordinates with the lowest binding energy were also used for further MD simulation (complex 2f, see below). The best docking mode obtained from Autodock Vina with small grid box was used as the starting structure (for MD simulation) named complex 1a. Another binding mode obtained with the larger grid box was used and named complex 3a. Additional starting structures complex 1b, 1c and 2a-2f were obtained from the Autodock 4.2 docking results. To obtain additional binding modes between the ligand and protein structures from MD simulation, NSC663284 was docked into 8 representative structures obtained from clustering of the apo protein MD simulations using Autodock Vina. (The apo protein MD simulation and clustering are described in the following section.) Among all eight docking modes obtained, one conformation was significantly different from those obtained by docking into the crystal structure, which was studied further as complex 2g.

Molecular dynamics simulations

The crystal structure of Cdc25B used as the starting structure for MD simulation was prepared as described above. For the NSC663284 ligand, partial atomic charges consistent with the Amber force-field used (RESP fitting of the HF/6-31G optimized structure) were calculated using the R.E.D server [35, 36]. GAFF force field parameters together with these charges were used for the ligand. To study the solution structure of the Cdc25B catalytic domain without inhibitor, the protein was also simulated without ligand (apo protein) [37]. The apo protein and the complexes obtained from docking were prepared for simulation using the Amber ff12SB force field for the protein [38-39] and solvation in a rectangular box of TIP3P water [40], with a minimum distance between the protein and the box edge of 11 Å. The crystal structure has

fewer residues defined at the C-terminus than the construct used for crystallisation (as well as the natural Cdc25B). Since the negative charge on the introduced Ala551 carboxylate terminus may influence the protein-ligand dynamics in site I, three different structures were built employing different C-terminal ends. The first C-terminal end was at Ala551 with a C-terminal carboxylate group (the apo system is hereafter referred to as '1qb0_OXT'). The second was modified with an N-methyl cap on the C-terminal Ala551 residue (the apo system is hereafter referred to as '1qb0_NME'). The third was built with two additional residues (Gly552 and Glu553 according to protein sequence), with Glu553 capped by an N-methyl group (the apo system is hereafter referred to as '1qb0_TWO'). Models with more residues were not considered because of the high uncertainty of the additional coordinates and the fact that the docking poses obtained would not be in contact with such additional residues. Gly552 and Glu553 were energy minimized for 1000 steps before performing the standard equilibration protocol as outlined below. All three receptor structures with different forms of C-terminal ends were used for further simulation. The total charge of the 1qbo_NME and 1qb0_TWO models was -1 and that of 1qb0_OXT was -2 . To neutralize the systems, one or two Na^+ counter ions were added. The complex structures are referred to by adding the relevant suffix "OXT/NME/TWO" (e.g. 1a_OXT).

Optimization and equilibration protocols were applied to all systems before running production MD simulation. Initial optimization of the solvent consisted of 1000 cycles of energy minimization followed by 50ps of MD simulation at 298K (applying a positional restraint of $100 \text{ kcal mol}^{-1} \text{ \AA}^{-2}$ on all solute atoms). The whole system was then optimized by 1000 cycles of energy minimization with a mild positional restraint on the protein $\text{C}\alpha$ atoms ($2.0 \text{ mol}^{-1} \text{ \AA}^{-2}$). All equilibration and production simulations were performed with the pmemd.cuda module and the default Mixed Single/Double/Fixed Point precision model. To prepare for production simulations, first, the temperature was increased from 50 to 298 K over a period of 50 ps

(maintaining the mild restraint on C α atoms). Second, 200 ps simulation in the NPT ensemble at 298 K and a pressure of 1 bar was performed, again maintaining the mild restraint on C α atoms. Thereafter, the whole system was briefly further equilibrated by 100 ps of NPT MD simulation (298 K, 1 bar). After this equilibration procedure, 50 ns MD simulation in the NPT ensemble at 298 K and 1 bar was carried out. Throughout, periodic boundary conditions were applied and the SHAKE algorithm was applied to fix all bond lengths involving hydrogen atoms. Temperature was maintained using langevin dynamics (collision frequency of 2 ps⁻¹) and pressure with the Berendsen barostat (pressure relaxation time of 1 ps). A time step of 2 fs was used, with a direct-space cut off radius of 8.0 Å for non-bonded interactions and particle-mesh Ewald for long-range electrostatic interactions. The trajectory was sampled every 2 ps (1000 steps intervals) for analysis. In total, three different apo protein systems and ten protein bound systems were simulated. Two independent runs were carried out for each system.

Analysis of molecular dynamics simulations

The AmberTools programs ptraj and cpptraj were used for trajectory analysis. Simulations were visualised using VMD (<http://www.ks.uiuc.edu/Research/vmd/>) [41]. The snapshots of two MD simulated trajectories of apo protein system 1qb0_OXT were clustered into 8 different clusters using Average Linkage and the root-mean-square of the C α atoms of the stable part of the structure as the distance metric (residues 388-412, 418-455, 465-494 and 504-551). Representative structures (cluster centroids) from the clusters with occurrence larger than 1% were considered in docking experiments (see above). The RMSF values of the apo protein systems were calculated after alignment on the average structure of the 50 ns trajectory. After aligning the C α atoms of the protein, the RMSD of the ligand heavy atoms with respect to the starting binding position was measured, in reference to the protein. Clustering of all stable protein-ligand trajectories was carried out on the distance between weight centres of atoms N, O and O1 on the ligand and the C α atoms of Cys426, Leu445 and Arg479 (Supplementary

figure S1). DSSP secondary structure assignment was performed using WORDOM [42, 43]. The definition of the measured distances between pairs of residues within the identified binding site is listed in Table S2.

Results and discussion

Flexibility of Cdc25B phosphatase and stability of the C-terminal helix

To investigate the solution structure and flexibility of the Cdc25B catalytic domain in absence of the ligand, several molecular dynamic simulations of 50 ns were carried out in explicit water, based on the crystal structure of the catalytic domain of human Cdc25B obtained at 1.9 Å resolution (PDB ID: 1QB0). Three different forms of the C-terminal end of the domain were considered: 1qb0_OXT – residues 374-551 with a C-terminal carboxylate; 1qb0_NME – residues 374-551 with an N-methylamide C-terminal cap; and 1qb0_TWO – residues 374-553 (Gly552 and Glu553 modelled on and an N-methylamide cap on Glu553 C-terminus). Overall, the structure of the Cdc25B domain remains stable during all simulations, except for the largely unstructured and flexible 6 C-terminal residues (8 for the 1qb0_TWO construct). The average C α RMSD values without the C-terminal residues for the final 25 ns of simulation range from 1.23 Å to 1.43 Å (apart for 1qb0_NME run 2, where the C-terminal helix shifts its position). The flexibility (root mean square fluctuation of C α atoms, RMSF) of the three constructs was similar, with the pattern in line with the *B*-factors of the crystal structure (Figure 2). Due to the absence of residues beyond the length of the simulated construct, high RMSF values were measured at the N- and C-terminal residues in all simulations (typically > 2 Å) as expected. RMSF values higher than for the remainder of the protein were also observed for residues 447-464 (1-2 Å). Higher flexibility of this region is expected, as it is the binding site of phosphate esters [44]. In some simulations, a change in position was also observed for the C-terminal

helix A (residues 534-546), which lies largely outside of the globular core of the Cdc25B catalytic domain (see Figure S2). This region is possibly disordered in Cdc25A [45] and a previous single 60 ns MD simulation of Cdc25B reported “a local unfolding and detachment from the protein main-body” for helix A in Cdc25B [22]. In our simulations, only a small positional shift of the helix A was observed occasionally, but no unfolding. The overall conformation of the Cdc25B catalytic domain in the simulations is thus very similar as the crystal structure, and reasonably stable. This is consistent with recent structural studies of Cdc25B that came to the same conclusions based on NMR measurements and molecular dynamics simulation [46, 47].

To further investigate the stability of the C-terminal helix A (defined in 1QB0.pdb as residues 534-546), the secondary structure of the last 19 residues (H533-A551) was determined for apo protein simulations with C-terminus of OXT and NME, as well as the last 21 residues (H533-E553) for C-terminus of TWO (Figure S3). For all three systems, region K537-K546 remains α -helical for the majority of the simulation time, and L540-F543 essentially the whole time. Residues H533-F536 show a 3_{10} -helix for about 10-30% of the 50 ns simulations. The last five residues T547-A551 do not show any regular secondary structure (apart from some helicity in 1qb0_NME run 2). These observations are in agreement with the NMR residual dipolar coupling measurements and molecular dynamics simulations of a Cdc25B protein construct that contains the C-terminal tail up to Q566 [47]. Our analysis thus indicates that the C-terminal helix is realistically stable in our truncated models, independent of the C-terminal cap at or beyond Ala551.

Initial binding modes identified by docking

NSC663284 was docked into the Cdc25B crystal structure (PDB ID: 1QB0) as well as representative structures from MD simulations. We define three major binding sites: site I, site

264 II and site III (Figure 3). Site I is a pocket between the C-terminal helix A and the P-loop, and
265 includes the site commonly referred to as the ‘swimming pool’. It does not face the catalytic
266 site directly. Site II is a shallow pocket above the P-loop. In contrast to site I, it allows direct
267 and close contact with the catalytic residue Cys473, and is therefore commonly referred to as
268 the ‘active site’. Both two sites have been mentioned by previous docking studies as potential
269 binding sites for quinolinedione inhibitors [22-26]. Site III is a pocket flanked by helix B and
270 several loops. It has been reported as the main region taking responsible protein-protein
271 interaction. The inhibitor 2-fluoro-4-hydroxybenzonitrile (referred as 3M8 in the following,
272 consistent with its residue name in PDB ID 4WH9) was reported to bind to this site recently
273 [48]. In order to clarify the whole binding mode identification process, the overall workflow is
274 described in Figure S4.

275 Molecular docking of NSC663284 was performed using the wild-type crystal structure (PDB
276 ID: 1QB0). All nine binding poses identified by AutoDock Vina suggest site I as the binding
277 site when the smaller grid box was applied. When the larger grid box was applied, the first
278 three and last two poses again suggest site I, but poses ranked 4-7 suggest site III as the binding
279 site. The conformation with the lowest predicted binding energy ($-6.6 \text{ kcal}\cdot\text{mol}^{-1}$ and -6.1
280 $\text{kcal}\cdot\text{mol}^{-1}$) were named complex 1a and 3a respectively. Both were used as the starting point
281 for further MD simulations (Figure 3). The binding poses identified by AutoDock 4.2 were
282 clustered into 13 clusters (Figure S5, Table S3). Cluster 1 and 4 suggest ligand binding to site
283 I (lowest binding energies of -3.28 and $-3.17 \text{ kcal mol}^{-1}$ respectively). However, cluster 3
284 (with the largest population size) suggests binding to site II (lowest binding energy of -3.19
285 kcal mol^{-1}). The best ranked conformations from the 7 highest populated clusters were prepared
286 for further MD simulation as complex 1b-c (for ligand binding in site I, Figure 3) and complex
287 2a-e (for ligand binding in site II, Figure 4). The binding conformations of clusters 9-11 are
288 similar, as are their populations (24, 22 and 27, respectively). The best ranked conformation

289 from cluster 11 was used for further MD simulation (complex 2f). Clusters 8, 12 and 13
290 (population of 1 or 2) were not considered further.

291 Complex 1b (from AutoDock 4.2) has a very similar conformation as complex 1a (from
292 AutoDock Vina). Complex 1c shares the same binding site with complexes 1a and 1b, but the
293 orientation of the quinolinedione ring and the tail moiety is different. Apart from complex 2f
294 and 2g, all poses in binding site II bind in the same position with the inhibitor interacting with
295 the P-loop, the short N-terminal loop of helix V and residues 392-394 of the catalytic domain.
296 The tail moiety of complex 2a interacts with site II directly with the quinolinedione ring
297 pointing outwards into solvent. Complexes 2b and 2e share a similar pose, with the
298 quinolinedione ring facing the protein and the tail moiety pointing outwards. The main
299 difference between 2b and 2e is that the quinolinedione ring is flipped. In complex 2d the
300 quinolinedione ring is turned by $\sim 90^\circ$ compared to 2b and 2e, and in complex 2c the tail moiety
301 instead of the quinolinedione ring is facing the protein. Finally, complex 2f shows a different
302 position of the ligand, with the quinolinedione ring close to catalytic residue Cys473 (distance
303 between atom C2 of NSC663284 and the thiolate sulphur of Cys473 is 3.7 Å).

304 Additional docking experiments were performed with structures obtained from MD simulation
305 of the apo protein. Clustering of the 1qb0_OXT simulations identified 6 different clusters, and
306 NSC663284 was docked into representative structures (cluster centroids) for each, using
307 Autodock Vina. In four cases, the best ranked binding modes were located in site I, and in two
308 cases, the best ranked binding modes were located in site II. All but one of these best ranked
309 binding modes was similar to the binding modes already obtained from docking into the crystal
310 structure (Table S4, Figure S6). The remaining binding mode was similar to that previously
311 reported by Arantes (1Dm) [22]. Thus, this mode was labelled complex 2g and used for further
312 investigation with MD simulation.

In summary, 11 complexes with NSC663284 were used as the starting points for MD simulation, three poses binding to site I (complex 1a-1c), seven binding to site II (complex 2a-2g) and one binding to site III (complex 3a). The 3 complexes that show the ligand binding to site I (complexes 1a-1c) include 1 pose suggested by Autodock Vina and 2 poses suggested by Autodock 4.2. Seven different docking complexes show the ligand binding in site II, including six obtained from docking with Autodock 4.2 to the crystal structure (complexes 2a-2f) and one obtained from docking with Autodock Vina to a representative structure from apo protein MD simulation (complex 2g). One further complex (obtained with a larger grid box for docking with AutoDock Vina) shows the ligand binding to site III (complex 3a).

Binding site identified by molecular dynamics simulation

To investigate whether the initial binding modes are stable, two 50ns MD simulations were performed for each of the 10 complexes selected from docking, using the CdC25B model with a carboxylate C-terminal end at residue Ala151 (OXT). Alongside visual inspection, displacement of NSC663284 from the starting point was quantified by aligning simulation snapshots to the C α atoms of CdC25B that do not show high flexibility (residues 388-412, 418-455, 465-494 and 504-545) and measuring the RMSD (without fitting) of the non-hydrogen atoms of the ligand (see Table 1, Figure S7). This measurement, obtained using the initial binding modes as reference, will be referred to as: 'ligand displacement RMSD'.

In four out of six simulations with the ligand starting in site I, the ligand does not leave the binding site in 50 ns of simulation. For complexes 1a and 1b, the ligand leaves in one run (run 2), but stays in the active site in approximately the same pose for the majority of the other (run 1, as indicated by ligand displacement RMSD values below 4 Å, Figure S7), with occasional small displacement (ligand displacement RMSD values around 4 Å, Figure S7). In runs 2, the

337 ligand moves away from the binding site after 20 and 17 ns of simulation for complex 1a and
338 1b, respectively (ligand displacement RMSD >6 Å, Figure S7). After the quinolinedione ring
339 leaves the shallow binding pocket, it initially maintains interaction with the C-terminal residues
340 146-151 (for 20 and 13 ns in 1a and 1b, respectively) before being released in solution
341 (indicated by ligand displacement RMSD increasing to above 10 Å, Figure S7). For complex
342 1c, the ligand displacement RMSD rises to about 6 Å at first but then stabilize around 4 Å after
343 10 ns in run 1 and 20 ns in run 2. Visual inspection confirms that the ligand adjusts its binding
344 mode in simulation away from complex 1c, but the ligand remains bound to binding site I
345 (Figure 5).

346 In all simulations of complexes 2a-2g (14 in total), the ligand rapidly moves away from its
347 initial binding pose (within 0-3 ns, indicated by ligand displacement RMSD >4 Å, Figure S8).
348 Also in all cases, the ligand moves out of site II completely within 15 ns (ligand displacement
349 RMSD ≥ 10 Å, Figure S8). In several cases, temporary binding to the protein surface occurs
350 (before or after release into solution), but the binding sites differ and binding never persists.
351 In one of the simulations of complex 2b, the ligand moves from site II into site I (see Figure
352 6). After 10 ns of simulation, the tail moiety has lost all contact with site II residues, and after
353 10 ns it forms interactions with F475. Once the quinolinedione ring has lost contact with F475
354 in site II after 12 ns, it forms interactions with Y428 and R482 after 15 ns, similar to the major
355 binding modes observed in simulations of the ligand bound to site I (see Figure 7 and next
356 section). After 35 ns, the ligand adopts a stable binding mode in site I with a hydrogen bonding
357 interaction between Y428 and the oxygen atom on quinolinedione ring. This binding mode
358 differs from the main binding modes identified, primarily due to the formation of a stacking
359 interaction with W550 that positions itself between the ligand and R482 (Figure 6, final panel).

360 In the simulation of complex 3a, the ligand moves away from its initial binding pose (within
361 30 ns, indicated by ligand displacement RMSD >4 Å, Figure S9A) in run1. In run2, the ligand

shifts a little out from the initial binding site from 8ns to 22ns, before moving back to its initial position. After 41 ns, however, the quinolinedione ring moves out of the pocket, now binding only with its tail moiety binding at the entrance of the pocket (figure S9C). The ligand could easily unbind completely once it adopts this pose (which is highly similar to the pose found in run1 prior to unbinding; figure S9B). It is possible that the quinolinedione ring is somewhat too big to bind stably in site III. Using the same docking and MD protocol, we investigated the co-crystallized inhibitor 3M8 (with smaller aromatic moiety than the quinolinedione ring) which was reported to binding on site III in crystalized structure (PDB ID: 4WH9). It showed very stable binding in site III in at least in one run (figure S11-S12).

In the starting structures of complex 1a, 1b and 1c, the quinolinedione ring points inward into the pocket (see Figure 5; complex 1b not show as it is very similar to complex 1a). The main surrounding residues (within 5 Å) are Arg482, Arg479, Met483, Tyr428, Glu478, Arg544 and Ser549. Of these, Arg482, Glu478 and Ser549 lie at the entrance of the pocket. Hydrogen bonds form between (one of the) two oxygen atoms of the quinolinedione ring and the donor atoms provided by Tyr428 and Arg482. Compared to the quinolinedione ring, the movement of the tail moiety shows much larger freedom in all simulations (see next section). In all simulations of complexes 1a, 1b and 1c where the ligand stays bound to the protein, the C-terminus, Arg482 and Glu478 approach each other, which leads to a more closed binding pocket.

In short, MD simulation indicates that stable ligand binding is only possible in site I. This is consistent with the preference for site I in docking (AutoDock Vina only returns binding poses in this site and AutoDock 4.2 predicts a marginally higher affinity). The preference for site I over site II is further illustrated by one of the simulations of complex 2a, where the ligand moves from site II to site I.

Characterization of the major binding mode in site I

386 In the initial MD simulations (see previous section), Ala551 was the C-terminal residue and
387 was simulated with a carboxylate terminus (OXT). Although Ala551 is the last residue
388 observed in the crystal structure (only the amide nitrogen), the crystallised construct of Cdc25B
389 extends to Gln566. The negative charge on the carboxylate terminus may influence the protein-
390 ligand dynamics in site I [45], so we performed additional simulations of the docked complexes
391 1a and 1c (1b is very similar to 1a, so was not included here). One set of simulations was
392 performed with a neutral N-methylated C-terminus (NME) and another with two additional
393 residues (Gly552 and Glu553, according to the sequence) as well as an N-methylated C-
394 terminus (TWO).

395 Four simulations of the complex_OXT system, two for the complex_NME system and three
396 for the complex_TWO system show stable binding of the ligand in site I (see Tables 1 and 2,
397 and also the ‘Ligand displacement RMSD’ in Figure S9). Generally, the tail moiety is more
398 flexible in these simulations and its conformation changes from the initial docked pose,
399 whereas the quinolinedione ring stays largely in place (see RMSD values of the quinolinedione
400 ring and the tail moiety in Figure 7). This observation is in line with the fact that various
401 compounds with a quinolinedione core structure but different tail moieties have been designed
402 as effective inhibitors for Cdc25B [9].

403 Because the tail moiety shows significant flexibility in the simulations, the position of the
404 quinolinedione ring was used to evaluate the binding modes. All snapshots from the
405 simulations of each complex system were clustered by calculating the distance between the
406 center of mass of the N, O and O1 atoms on the ligand (see Figure 7) and the center of mass of
407 the C_α atoms of Cys426, Leu445 and Arg479 (Figure S1). This revealed a major binding mode,
408 mode A (Figure 7a), which is mainly observed in simulations of complex 1a and 1b in all three
409 N-terminal variants (OXT, NME and TWO; see Table 3). For complex 1c_OXT, the first
410 several nanoseconds of both simulations also show mode A. After that, the ligand adopts

411 binding modes which are not clustered into mode A, although the ligand returns to binding
412 mode A in the last 5 ns in one case. The situation is similar for the simulations of 1c_NME and
413 1c_TWO, with the notable exception of one run of complex 1c_NME, where the ligand quickly
414 changes to mode A and then stays in that binding mode for the majority of the simulation.

415 Binding mode A is characterized by possible hydrogen bond interactions between the ligand
416 and Tyr428, Arg482, Thr547 and Ser549 (see Figure 7A). In all frames clustered as binding
417 mode A, the occurrence of these four interactions is 64.0%, 56.8%, 35.7% and 27.1%
418 respectively (distance cut-off of 3.5 Å, angle cut off of 45°). Clearly, the two oxygen atoms on
419 the quinolinedione ring play an important role in binding in this mode. No specific interaction
420 is found with the Cl atom of the ligand, in accordance with the observation that absence of the
421 Cl substituent does not significantly influence inhibition [20].

422 A second (minor) binding mode, mode B, was primarily observed in the simulation of complex
423 1c_TWO. This mode is present for more than 95% of this simulation, but was not found in the
424 simulations of complex1a_TWO. Mode B is similar to binding mode A (Figure 7B), but no
425 clear hydrogen bond interactions are formed between the quinolinedione oxygen atoms and
426 Tyr428 and Arg482. The quinolinedione ring is in a position to form a π - π interaction with
427 Tyr428, and perhaps an additional (cation- π) interaction with the guanidinium moiety of
428 Arg482. The fact that mode B was only found in the complex_TWO system is likely due to a
429 slight conformational change of the terminal helix A: the last several residues (two of which
430 are only present in the complex_TWO systems) move ‘upwards’ towards helix A instead of
431 interacting with Arg482. The last 16 residues of the full construct (A551-Q566) are not
432 observed in the crystal structure [17] and NMR data indicate that the final 20 residues (S549-
433 Q566) are disordered, but can form transient contact with the rest of the protein [46]. The
434 observed change in position of the final C-terminal residues in the complex_TWO system may
435 therefore be relevant, which can lead to binding mode B.

Previously, binding modes of NSC663284 and Cdc25B were suggested based on extensive docking studies [19]. One possible mode (suggested by AutoDock 4) indicated the quinolinedione ring hydrogen bonding to Arg482 and Arg544 and the tail moiety positioned near the P-loop. Another possible mode (in the opposite orientation, suggested by Gold) indicated the quinolinedione ring positioned near the P-loop and the tail moiety placed between Arg544 and Arg482. The authors suggested that the first possible mode was more likely as the ligand binds closer to the catalytic residue Cys473. Although the major mode suggested here (mode A, figure 7A) also features interactions with Arg482, the position/orientation is different. We obtained a binding mode through docking similar to the mode suggested in ref. [19] (complex 2f), but MD simulation indicates that this binding mode is not very stable.

The mode of action of quinolinedione molecules on Cdc25B is not yet clear. Sulfhydryl arylation of Cys473 was shown unlikely to be the main inhibition mechanism [49]. Previously, quinolinediones have been reported to inhibit Cdc25B through redox cycling and production of H₂O₂, leading in turn to the irreversible oxidation of Cys473 [20]. Such an indirect mechanism does not explain, however, the differences in inhibition observed for quinolinediones with different substituents leading to changes in steric and electronic properties [15, 22]. The latter indicates that binding of quinolinediones to Cdc25B probably does play a role, although a direct connection between the quinolinedione ring and the active site Cys473 may not be necessary to explain the inhibition. Four arginine residues (Arg479, Arg482, Arg544 and Arg548) are in the vicinity of the catalytic Cys473, and may be involved in the initial binding of the substrate phosphate moiety. In the model of the Cdk2–CycA complex binding to Cdc25B suggested by Sohn *et al.* [50], Arg479 (which is closest to the catalytic residue Cys473) interacts directly with the phosphate. In our suggested binding mode A, the ligand directly interacts with Arg482. The presence of the ligand further prevents free movement of Arg479. The tail moiety further forms transient interactions with residues on

helix A, including Arg544 and Arg548. The overall pose is similar to that suggested by molecular docking for a naphthofurandione inhibitor that showed competitive inhibition of Cdc25B (3-benzoyl-naphtho[1,2-b]furan-4,5-dione or 5169131) [51].

Notably, the binding of NSC663284 leads to some small, but significant, changes in the structure and interactions of residues around its binding site (see Supporting Information). These changes and the presence of NSC663284 are likely to affect the protein-protein interactions between Cdc25B and its protein substrates [49], in a similar fashion as recently reported for small molecules developed through screening of small-fragment like compounds using NMR chemical shift perturbations [52].

Conclusions

Through the use of docking and extensive MD simulations, we have identified the likely binding site of NSC663284 and related quinolinedione inhibitors to the Cdc25B phosphatase. Initially, 11 possible complexes were obtained by using different docking programs (and different grid boxes and docking in the crystal structure as well as structures sampled from MD simulation. In three complexes, the ligand is located in the so-called ‘swimming pool’, as site between the P-loop and helix A (here labelled site I). Seven complexes present binding modes with the ligand near the catalytic cysteine (site II) and one complex has the ligand binding in a region known to be involved in protein-protein interaction (site III). Several 50 ns MD simulations (at least 2 per complex) show that stable binding of the ligand only occurs in site I. Clustering identified the likely binding mode of NSC663284, which includes hydrogen bonding of the quinolinedione oxygens with residues Tyr428 and Arg482. This binding mode was shown to be largely independent of the treatment of the C-terminal residues in the simulation (where the unstructured C-terminal part of Cdc25B starts). Interactions between the ligand and Cdc25B lead to a limitation of the freedom around the binding pocket, which in

turn is likely to affect binding of the protein substrate, leading to the observed inhibition of quinolinedione compounds. The identification of the quinolinedione binding site will assist in structure-based drug design of effective inhibitors against Cdc25B, an important target for anti-cancer therapies.

Acknowledgements

The authors would like to thank Dr. C. J. Woods for helpful discussion and advice. YG and YL acknowledge financial support from National Science Found for Distinguished Young Scholars of China (21225313), Program for Changjiang Scholars and Innovative Research Team in University (IRT1030). Major State Special Research Project of China (2016YFA0101200), Major State Basic Research Development Program of China (973 Program, 2015CB553701), National Natural Science Foundation of China (NSFC, 21778050). MWvdK and AJM thank BBSRC and EPSRC for support (EP/G007705/1; BB/L018756/1; BB/M026280).

References

1. Boutros R, Lobjois V, Ducommun B (2007) Cdc25 phosphatases in cancer cells: key players? Good targets? *Nat Rev Cancer* 7:495-507.
2. Munter SD, Köhn M, Bollen M (2013) Challenges and opportunities in the development of protein phosphatase-directed therapeutics. *ACS Chem Biol* 8:36–45.
3. Boutros R, Dozier C, Ducommun B (2006) The when and the wheres of Cdc25 phosphatases. *Curr Opin Cell Biol* 18:185–191.
4. Van Vugt MA, Bras A, Medema RH (2004) Polo-like kinase-1 controls recovery from a G2 DNA damage-induced arrest in mammalian cells. *Mol Cell* 15:799–811.
5. Bugler B, Quaranta M, Aressy B, Brezak MC, Prevost G, Ducommun B (2006) Genotoxic-activated G2-M checkpoint exit is dependent on Cdc25B phosphatase expression. *Mol Cancer Ther* 5:1446-1451.

- 511 6. Neely KE, Piwnica-Worms H (2003) Cdc25A regulation: to destroy or not to destroy—is that
512 the only question? *Cell Cycle* 2: 455-457.
- 513 7. Ferguson AM, White LS, Donovan PJ, Piwnica-Worms H (2005) Normal cell cycle and
514 checkpoint responses in mice and cells lacking cdc25b and cdc25c protein phosphatases.
515 *Mol Cell Biol* 25:2853–2860.
- 516 8. Guo JC, Kleeff J, Li JS, Ding JY, Hammer J, Zhao YP, Giese T, Korc M, Buchler MW,
517 Friess H (2004) Expression and functional significance of CDC25B in human pancreatic
518 ductal adenocarcinoma. *Oncogene* 23:71-81.
- 519 9. Marie-Odile Contour-Galcerà, Sidhu A, Prévost G, Bigg D, Ducommun B (2007) What's
520 new on CDC25 phosphatase inhibitors. *Pharmacol Ther* 115:1-12.
- 521 10. Lavecchia A, Giovanni CD, Novellino E (2010) Inhibitors of Cdc25 phosphatases as
522 anticancer agents: a patent review. *Expert Opin Ther Patents* 20:405-425.
- 523 11. Lavecchia A, Di Giovanni C, Novellino E (2009) Cdc25A and B dual-specificity phosphatase
524 inhibitors: potential agents for cancer therapy. *Curr Med Chem* 16:1831-49.
- 525 12. Lazo JS, Aslan DC, Southwick EC, Cooley KA, Ducruet AP, Joo B, Vogt A, Wipf P (2001)
526 Discovery and biological evaluation of a new family of potent inhibitors of the dual
527 specificity protein phosphatase cdc25. *J Med Chem* 44:4042-4049.
- 528 13. Guo JX, Parise RA, Joseph E, Lan J, Pan SS, Joo B, Egorin MJ, Wipf P, Lazo JS, Eiseman
529 JL (2007) Pharmacology and antitumor activity of a quinolinedione cdc25 phosphatase
530 inhibitor da3003-1 (nsc 663284). *Anticancer Res* 27:3067-3074.
- 531 14. Lavecchia A, Giovanni CD, Pesapane A, Montuori N, Ragno P, Martucci NM, Masullo M,
532 Vendittis ED, Novellino E (2012) Discovery of new inhibitors of cdc25b dual specificity
533 phosphatases by structure-based virtual screening. *J Med Chem* 55:4142-4158.
- 534 15. Cossy J, Belotti D, Brisson M, Skoko JJ, Wipf P, Lazo JS (2006) Biological evaluation of
535 newly synthesized quinoline-5,8-quinones as Cdc25B inhibitors. *Bioorg Med Chem*
536 14:6283–6287.
- 537 16. Wardman P (1990) Bioreductive activation of quinones: redox properties and thiol
538 reactivity. *Free Radic Res Commun* 8:219–229.
- 539 17. Reynolds RA, Yem AW, Wolfe CL, Deibel Jr MR, Chidester CG, Watenpaugh KD (1999)
540 Crystal Structure of the Catalytic Subunit of Cdc25B Required for G2/M Phase Transition
541 of the Cell Cycle. *J Mol Biol* 293:559-568.
- 542 18. Rudolph R (2007) Cdc25 phosphatases: structure, specificity, and mechanism. *Biochem*
543 46:3595-3603.

- 544 19. Buhrman G, Parker B, Sohn J, Rudolph J, Mattos C (2005) Structural mechanism of
545 oxidative regulation of the phosphatase Cdc25B via an intramolecular disulfide bond.
546 Biochem 44:5307-5316.
- 547 20. Jackson MD, Denu JM (2001) Molecular reactions of protein phosphatases: Insights from
548 structure and chemistry. Chem Rev 101:2313-2340.
- 549 21. Lavecchia A, Cosconati S, Limongelli V, Novellino E (2006) Modeling of Cdc25B dual
550 specificity protein phosphatase inhibitors: docking of ligands and enzymatic inhibition
551 mechanism. ChemMedChem 1:540-550.
- 552 22. Brisson M, Nguyen T, Wipf P, Joo B, Day BW, Skoko JS, Schreiber EM, Foster C, Bansal
553 P, Lazo JS (2005) Redox regulation of Cdc25B by cell-active quinolinediones. Mol
554 Pharmacol 68:1810-1820.
- 555 23. Arantes GM (2010) Flexibility and inhibitor binding in Cdc25 phosphatases. Proteins
556 78:3017-3032.
- 557 24. Park H, Carr BI, Li MH, Ham SW (2007) Fluorinated NSC as a Cdc25 inhibitor. Bioorg
558 Med Chem Lett 17:2351-2354.
- 559 25. Ko S, Lee W, Lee S, Park H (2008) Nanosecond molecular dynamics simulations of Cdc25B
560 and its complex with a 1,4-naphthoquinone inhibitor: Implications for rational inhibitor
561 design. J Mol Graph Model 27:13-19.
- 562 26. Braud E, Goddard ML, Kolb S, Brun MP, Mondésert O, Quaranta M, Gresh N, Ducommun
563 B, Garbay C (2008) Novel naphthoquinone and quinolinedione inhibitors of CDC25
564 phosphatase activity with antiproliferative properties. Bioorg Med Chem 16:9040-9049.
- 565 27. Lengauer T, Rareyt M (1996) Computational methods for biomolecular docking. Curr Opin
566 Struct Biol 6:402-406.
- 567 28. Brooijmans N, Kuntz ID (2003) Molecular recognition and docking algorithms. Annu. Rev.
568 Biophys. Biomol. Struct 32:335-373.
- 569 29. Coupez B, Lewis RA (2006) Docking and scoring - Theoretically easy, practically
570 impossible? Curr Med Chem 13:2995-3003.
- 571 30. SYBYL Software, Verison 8.1, St. Louis, Tripos Associates Inc., MO, USA, 2008.
- 572 31. Anandakrishnan R, Aguilar B, Onufriev AV (2012) H++ 3.0: automating pKa prediction
573 and the preparation of biomolecular structures for atomistic molecular modeling and
574 simulation. Nucleic Acids Res 40:537-541.
- 575 32. Morris GM, Huey R, Lindstrom W, Sanner MF, Belew RK, Goodsell DS, Olson AJ (2009)
576 Autodock4 and AutoDockTools4: automated docking with selective receptor flexibility. J
577 Comput Chem 16:2785-2791.

- 578 33. Trott O, Olson AJ (2010) AutoDock Vina: improving the speed and accuracy of docking
579 with a new scoring function, efficient optimization and multithreading. *J Comput Chem*
580 31:455-461.
- 581 34. Goodsell DS, Morris GM, Olson AJ (1996) Automated docking of flexible ligands:
582 applications of autodock. *J Mol Recognition* 9:1-5.
- 583 35. Vanquelef E, Simon S, Marquant G, Garcia E, Klimerek G, Delepine JC, Cieplak P,
584 Dupradeau FY (2011) R.E.D. Server: a web service for deriving RESP and ESP charges and
585 building force field libraries for new molecules and molecular fragments. *Nucl Acids Res*
586 39:511-517.
- 587 36. Bayly CI, Cieplak P, Cornell W, Kollman PA (1993) A well-behaved electrostatic potential
588 based method using charge restraints for deriving atomic charges: the RESP model. *J Phys*
589 *Chem* 97:10269-10280.
- 590 37. Wang J, Wolf RM, Caldwell JW, Kollman PA, Case DA (2004) Development and testing
591 of a general amber force field. *J Comput Chem* 25: 1157-1174.
- 592 38. Salomon-Ferrer R, Case DA, Walker RC (2013) An overview of the Amber biomolecular
593 simulation package. *WIREs Comput Mol Sci* 3:198-210.
- 594 39. Jorgensen WL, Chandrasekhar J, Madura JD, Impey RW, Klein ML (1983) Comparison of
595 simple potential functions for simulating liquid water. *J Chem Phys* 79:926–935.
- 596 40. Case DA, Darden TA, Cheatham TE, Simmerling CL, Wang J, Duke RE, Luo R, Walker
597 RC, Zhang W, Merz KM, Roberts B, Hayik S, Roitberg A, Seabra G, Swails J, Goetz AW,
598 Kolossváry I, Wong KF, Paesani F, Vanicek J, Wolf RM, Liu J, Wu X, Brozell SR,
599 Steinbrecher T, Gohlke H, Cai Q, Ye X, Wang J, Hsieh MJ, Cui G, Roe DR, Mathews
600 DH, Seetin MG, Salomon-Ferrer R, Sagui C, Babin V, Luchko T, Gusarov S, Kovalenko
601 A, Kollman PA. AMBER 12. University of California, San Francisco. 2012.
- 602 41. Humphrey W, Dalke A, Schulten K (1996) VMD - Visual Molecular Dynamics. *J Molec*
603 *Graphics* 14:33-38.
- 604 42. Seeber M, Cecchini M, Rao F, Settanni G, Caflisch A (2007) Wordom: a program for
605 efficient analysis of molecular dynamics simulations. *Bioinformatics* 23:2625–2627.
- 606 43. Kabsch W, Sander C (1983) Dictionary of protein secondary structure: pattern recognition
607 of hydrogen-bonded and geometrical features. *Biopolymers* 22:2577-2637.
- 608 44. Arantes GM (2008) The catalytic acid in the dephosphorylation of the Cdc2-pTpY/CycA
609 protein complex by Cdc25B phosphatase. *J Phys Chem B* 112:15244-15247.

- 610 45. Fauman EB, Cogswell J, Lovejoy B, Rocque WJ, Holmes W, Montana VG, Piwnica-Worms
611 H, Rink MJ, Saper MA (1998) Crystal structure of the catalytic domain of the human cell
612 cycle control phosphatase, Cdc25A. *Cell* 93:617-25.
- 613 46. Lund G, Cierpicki T (2014) Solution NMR studies reveal no global flexibility in the catalytic
614 domain of Cdc25B. *Proteins* 82:2889–2895.
- 615 47. Sayegh RSR, Tamaki FK, Marana SR, Salinas RK, Arantes GM (2016) Conformational
616 flexibility of the complete catalytic domain of Cdc25B phosphatases. *Proteins*. 84: 1567-
617 1575.
- 618 48. Lund G, Dudkin S, Borkin D, Ni W, Grembecka J, Cierpicki T (2014). Inhibition of
619 CDC25B phosphatase through disruption of protein–protein interaction. *ACS chemical*
620 *biology*. 10(2): 390-394.
- 621 49. Pu L, Amoscato AA, Bier ME, and Lazo JS (2002) Dual G1 and G2 phase inhibition by a
622 novel, selective Cdc25 inhibitor 7-chloro-6-(2-morpholin-4-ylethylamino)-quinoline-5,8-
623 dione. *J Biol Chem* 277:46877–46885.
- 624 50. Sohn J, Parks JM, Buhrman G, Brown P, Kristjansdottir K, Safi A, Edelsbrunner H, Yan
625 WT, Rudolph J (2005) Experimental validation of the docking orientation of Cdc25 with its
626 Cdk2-CycA protein substrate. *Biochem* 44:16563-16573.
- 627 51. Brisson M1, Nguyen T, Vogt A, Yalowich J, Giorgianni A, Tobi D, Bahar I, Stephenson
628 CR, Wipf P, Lazo JS (2004) Discovery and characterization of novel small molecule
629 inhibitors of human Cdc25B dual specificity phosphatase. *Mol Pharmacol* 66:824-833.
- 630 52. Lund G, Dudkin S, Borkin D, Ni W, Grembecka J, Cierpicki T (2015) Inhibition of CDC25B
631 phosphatase through disruption of protein-protein interaction. *ACS Chem Biol* 10:390-394.

Figure Legends

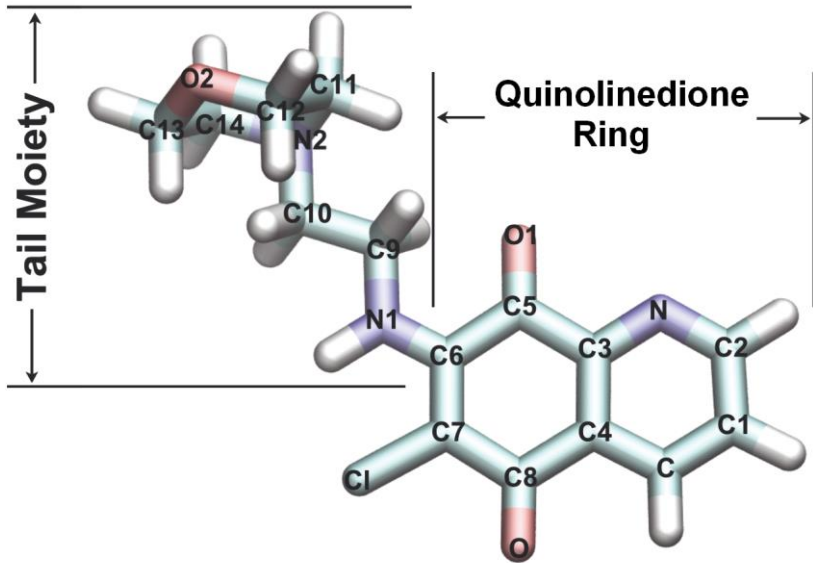


Fig.1. Chemical structure of NSC663284 with the atom and moiety names used in this study.

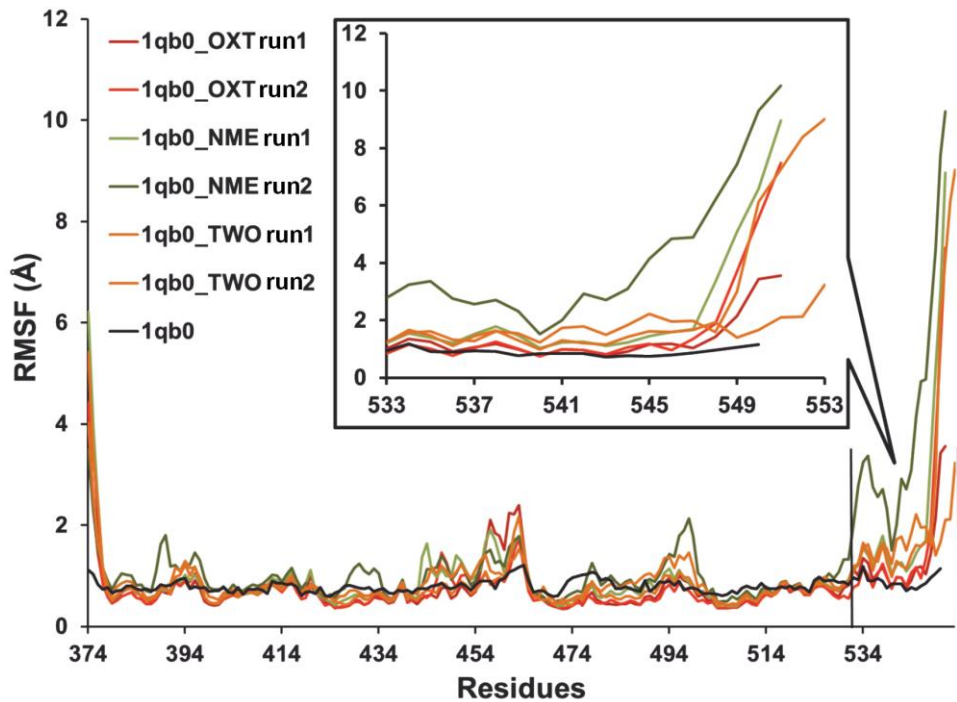


Fig.2. C_{α} root mean square fluctuations (RMSF) of the apo protein measured from 50ns MD simulations of the three C-terminal constructs (1qb0_OXT, 1qb0_NME and 1qb0_TWO), as well as the value calculated from the temperature (B) factors of the Cdc25B crystal structure (PDB ID: 1QB0).

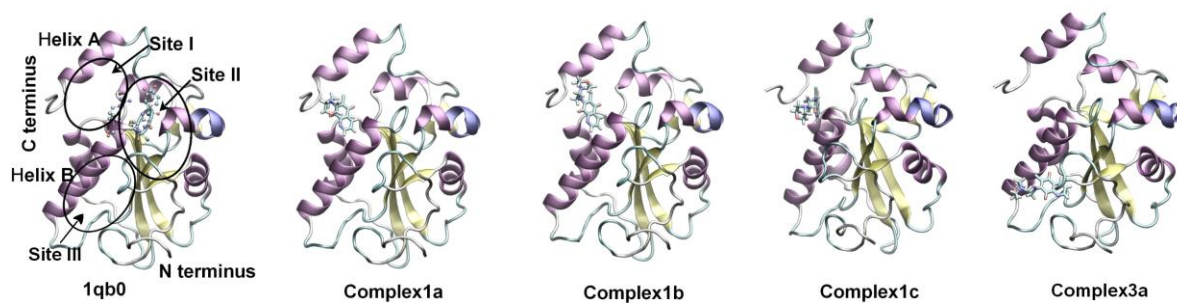


Fig.3. Schematic location of three binding sites in the protein (left) and four complexes with NSC663284 located in site I and site III obtained from docking. The protein backbone is shown as cartoon, the ligand as sticks. In the left panel, P-loop residues (without hydrogen atoms) are shown in ball and stick.

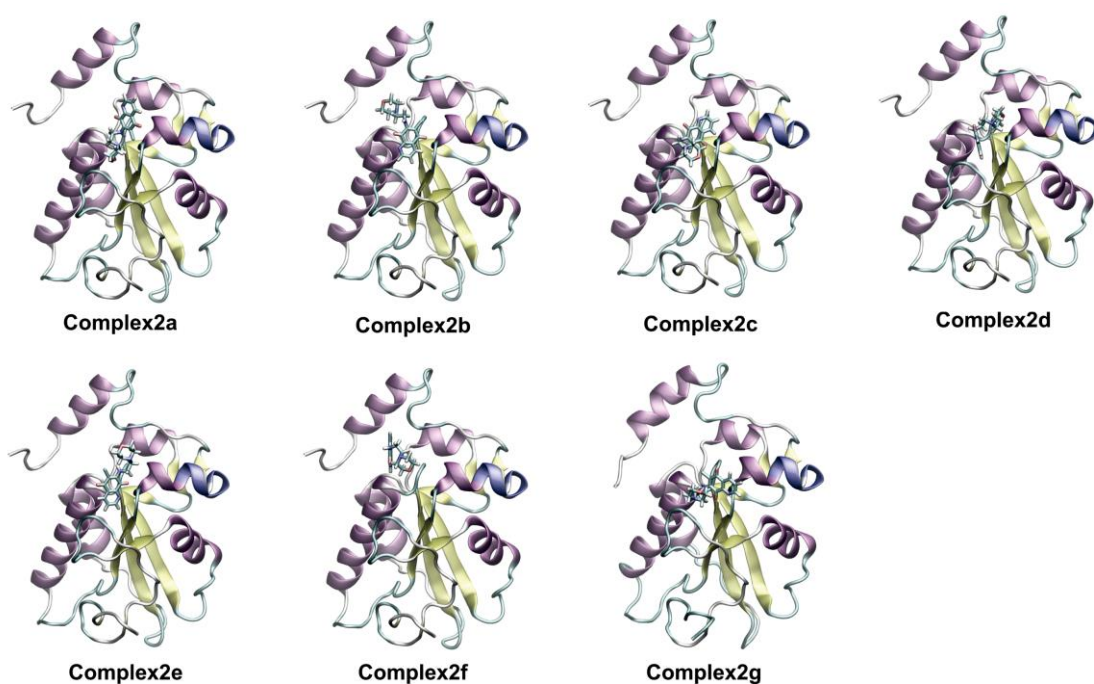


Fig.4. Seven complexes with NSC663284 located in Site II, obtained from docking. The protein backbone is shown as cartoon, the ligand as sticks.

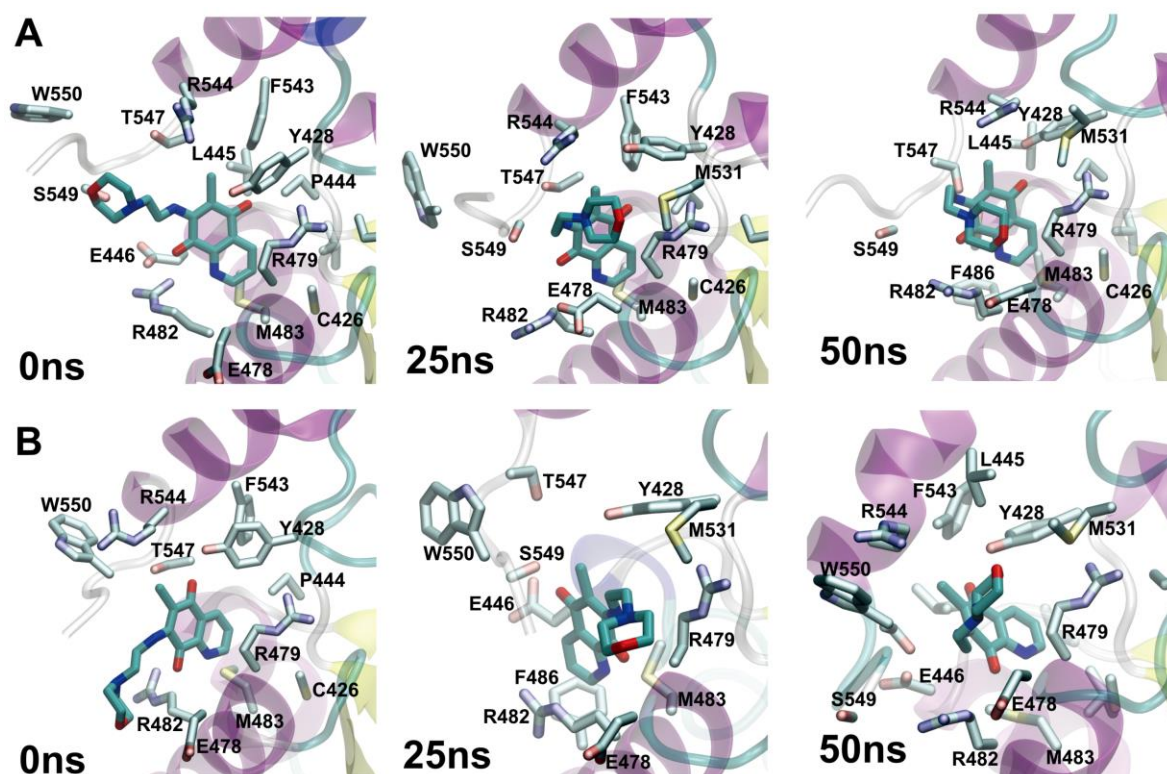


Fig.5. Snapshots of MD simulations of (A) complex 1a and (B) complex 1c at 0ns, 25ns and 50ns. The NSC663284 ligand and protein residues within 5 Å of the ligand are shown as sticks, without hydrogen atoms (for clarity).

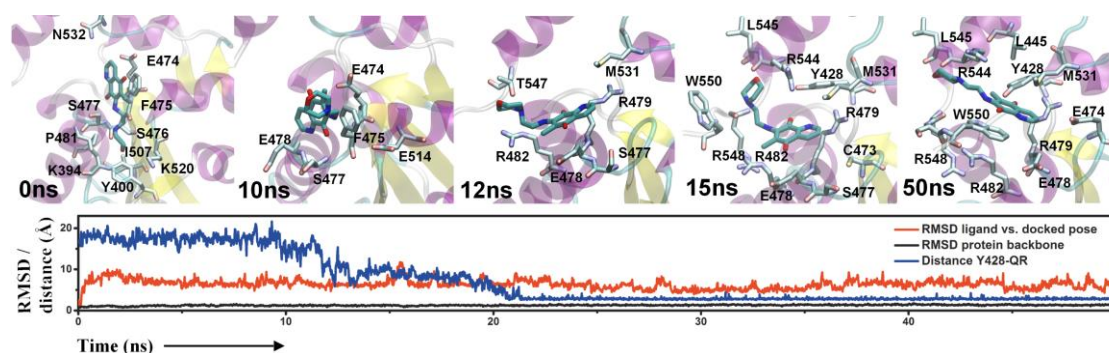


Fig.6. Movement of ligand from site II to site I. Snapshots of one simulation of complex 2a at 0, 10, 12, 15 and 50ns (top panels); RMSD of protein backbone, RMSD of ligand heavy atoms (after fitting on protein backbone) and the distance between Y428 and the oxygen atom O on the quinolinedione ring (bottom). The snapshots illustrate movement of the ligand from site II (0 ns) to site I (15 ns onwards). The ligand and protein residues within 5 Å of the ligand are shown as sticks, without hydrogen atoms (for clarity).

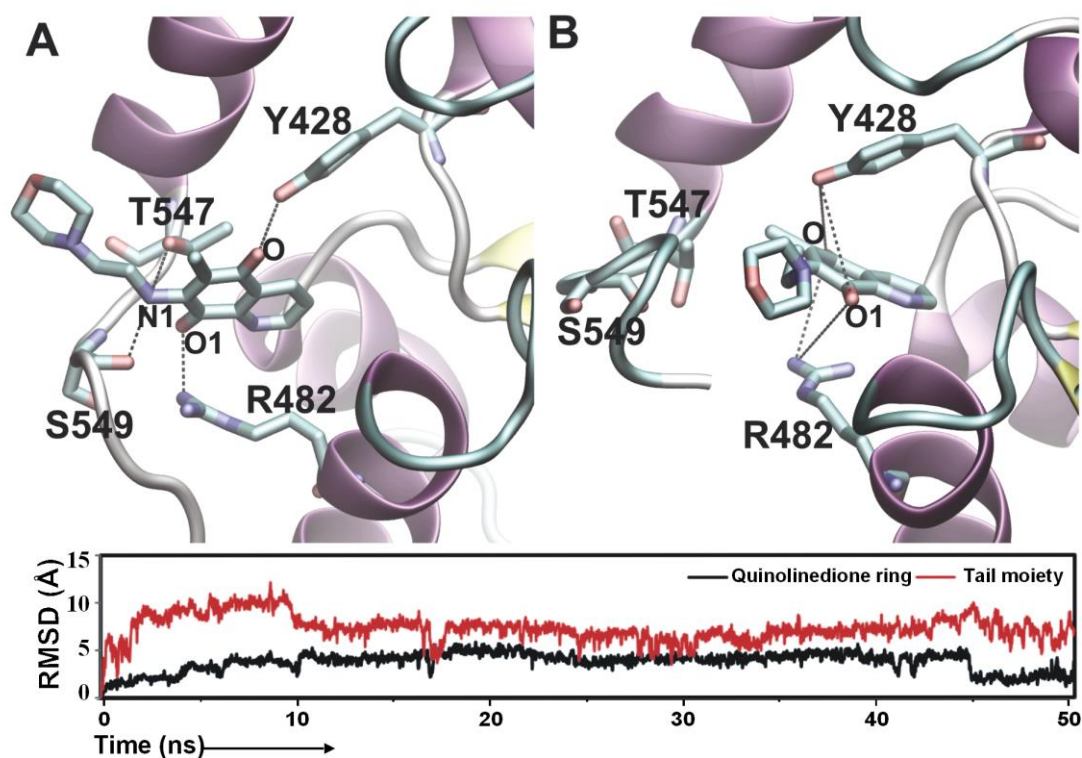


Fig.7. Interaction between NSC663284 and Cdc25B in the main binding modes identified. A: binding mode A; B: binding mode B. Graph below: backbone RMSD of the quinolinedione ring and tail moiety of the ligand during complex 1a_OXT simulation. The protein structure is displayed in cartoon, coloured by secondary structure; ligand and residues are displayed as sticks, without hydrogen atoms.

Tables

Table 1. Ligand binding during 25-50ns MD simulation of all 10 complexes (construct OXT).

	Site I			Site II						
Complex	1a	1b	1c	2a	2b	2c	2d	2e	2f	2g
Run 1	+	+	+	-	-	-	-	-	-	-
Average RMSD ^a	1.9	2.4	3.6	16.7	5.6	23.3	28.9	16.5	40.2	28.3
Run 2	-	-	+	-	-	-	-	-	-	-
Average RMSD ^a	34.8	10.7	4.4	11.0	27.0	31.5	29.4	25.0	19.3	28.6

+ Ligand in the site at the end of the simulation

- Ligand out of the site at the end of the simulation

^a Ligand displacement RMSD in Å: RMSD of ligand non-hydrogen atoms from the initial docked pose after alignment on protein Cα atoms, see text.

Table 2. Ligand binding in 25-50ns of MD simulation of the additional simulations with adjusted C-terminus (constructs NME and TWO).

	NME		TWO	
Complex	1a	1c	1a	1c
Run 1	-	+	-	+
Average RMSD ^a	18.1	2.4	9.8	7.2
Run 2	-	+	+	+
Average RMSD ^a	11.6	4.9	4.7	4.1

+ Ligand in the site at the end of the simulation

- Ligand out of the site at the end of the simulation

^a Ligand displacement RMSD in Å: RMSD of ligand non-hydrogen atoms from the initial docked pose after alignment on protein Cα atoms, see text.

Table 3. The distribution and occurrence of binding mode A in the nine MD trajectories where NSC663284 stays bound to CdC25B in site I.

C-terminal Construct	Distribution	Occurrence	Total occurrence by weight
OXT	1a_1>95%; 1b_1>95%; 1c_1: 0-4.2; 44.6-50.0 ns; 1c_2: 0-5.32 ns	59.0%	49.3%
NME	1c_1>95%; 1c_2: 0-7.94 ns	53.5%	
TWO	1c_1: 0-3.16 ns; 1c_2: 0-0.86 ns; 1a_2>95%	31.9%	